

Optical Response of Multi-orbital Superconductors: Role of Fermi Surface Topology and Geometry

Meghdad Yazdani-Hamid,¹ Mehdi Biderang,^{2,3} and Alireza Akbari⁴

¹*Department of Physics, Bu-Ali Sina University, 65178, 016016, Hamedan, Iran*

²*Department of Physics, University of Toronto, 60 St. George Street, Toronto, Ontario, M5S 1A7, Canada*

³*DelQuanTech Inc., 500 Doris Ave., Toronto, Ontario, M2N 0C1, Canada*

⁴*Beijing Institute of Mathematical Sciences and Applications (BIMSA), Huairou District, Beijing 101408, China*

(Dated: January 27, 2025)

Motivated by the possibility of shifting the nearest peak in the density of states relative to the Fermi level leading to a Lifshitz transition, such as through strain in Sr_2RuO_4 , this study examines the consequent effects on Hall transport and the polar Kerr angle. Using a three-orbital model, variations in the chemical potential and z -direction hopping reveal $d + ig$ - and $d_{x^2-y^2}$ -wave pairings as leading candidates for pairing symmetry in the quasi-2D orbital within the weak-coupling regime. The Lifshitz transition is further analyzed for its impact on coherence factors and the density of states, both of which are crucial to response functions. Interactions with van Hove points and nearby degenerate electronic states emerge as key contributors to Hall-type responses, while electron transfer between quasi-1D and quasi-2D orbitals significantly modifies these transport properties.

I. INTRODUCTION

Strontium ruthenate, a transition metal oxide with enigmatic superconducting symmetry, continues to captivate researchers due to its intricate interplay of orbital physics, electronic structure, and symmetry-breaking phenomena [1, 2]. As a prime candidate for studying strongly correlated electron systems, Sr_2RuO_4 provides a unique platform to explore the mechanisms behind superconductivity and its potential applications in advanced technologies [3–5]. However, achieving a detailed understanding of its electronic behavior remains a central goal, with particular emphasis on how variations in Fermi surface topology, chemical potential, and interorbital coupling shape its superconducting and transport properties [6, 7]. For instance, external perturbations such as strain can significantly tune the electronic structure, modifying the density of states (DOS), inducing Lifshitz transitions, and enhancing the superconducting transition temperature [8–10]. Moreover, they can modify the magnetic properties by adjusting the Ru-O-Ru bond angles and distances, impacting exchange interactions and the spin fluctuation spectrum [11–16]. These effects, driven by alterations in the electronic DOS and Fermi surface topology, underscore the potential of external perturbations to uncover and manipulate the fundamental physics of this material [17]. Furthermore, modifications in the Fermi surface topology can also be achieved by rotating the RuO_6 octahedra [18, 19], increasing the chemical potential [20], substituting La for Sr [21, 22], or utilizing SrRuO_3 - SrTiO_3 heterostructures [23].

On the other hand, a variety of experimental observations suggest the presence of time-reversal symmetry breaking (TRSB) in the superconducting state of Sr_2RuO_4 , pointing to the condensation of multiple superconducting order parameters, likely associated with two-dimensional irreducible representations of the D_{4h} crystal symmetry group [2, 6, 24, 25]. One of the key pieces of evidence for TRSB pairing is the Hall-type effects, which involves the generation of a transverse voltage in response to an applied current, even in the absence of an external magnetic field. Following this, the Kerr rotation effect has also been observed, where circularly polar-

ized light incident on the superconducting sample is reflected with its polarization rotated [26]. Despite these findings, the precise origins of both the Hall-type and Kerr effects in superconducting Sr_2RuO_4 remain a topic of ongoing debate, often being explored alongside questions about the dominant superconducting orbitals in the material. Extensive research has explored Hall transport and the polar Kerr effect using diverse approaches [27–39], often inspired by the primitive experimental evidences [26]. It has also been showed that the Hall response originates from the breaking of time-reversal symmetry in the gap function of the quasi-1D orbitals [38]. This highlights that spin-orbit coupling (SOC) plays a key role in mixing these orbitals, while the quasi-2D orbital has a minimal impact on this transport. Based on these findings, this study aims to examine the influence of the Lifshitz transition, closely linked to the quasi-2D orbital, on the Hall response governed by the quasi-1D orbitals.

Here, we aim to uncover the mechanisms behind the superconductivity of strontium ruthenate and explore methods to tailor its properties for applications in advanced electronics [40–43]. Our primary focus is investigating how variations in the Fermi surface of the γ band, especially its proximity to or distance from the Brillouin zone boundary, influence the coherence factor, density of states, and Hall transport. We employ a two-dimensional three-orbital tight-binding model combined with a self-consistent Bogoliubov-de Gennes approach. These effects are studied by tuning the chemical potential and enhancing the coupling between the quasi-2D and quasi-1D orbitals. This coupling is modeled through z -direction hopping, which, at a specific value, results in two nearly degenerate states near the Fermi level, causing changes in the band fillings of the corresponding degenerate bands near the Fermi energy. We begin by examining the leading candidate for the pairing symmetry on the quasi-2D orbital, the d_{xy} orbital, within the weak-coupling regime. Next, we shift our focus to the core theme of this paper: investigating the impact of the Lifshitz transition on Hall transport driven by the quasi-1D orbitals. In the following section, we introduce the physical model used to describe the electronic band structure and superconducting ground state, highlighting the favored pairing channel on the quasi-2D orbital within the weak-coupling

limit. Sections III and IV focus on calculating the dynamical Hall conductivity and the polar Kerr angle, utilizing the superconducting gap functions derived in Section II and a two-orbital model for the longitudinal conductivity. Finally, the concluding section summarizes the key findings and closes the paper.

II. MODEL HAMILTONIAN

The Hamiltonian of a 2D systems spread in xy -plane describing the normal state of strontium ruthenate is given by

$$\mathcal{H}_N = \sum_{\mathbf{k}, \nu, \nu', \sigma} (\xi_{\nu}^{\mathbf{k}} \delta_{\nu, \nu'} + \mathcal{T}_{\nu, \nu'}^{\mathbf{k}}) d_{\mathbf{k}, \nu, \sigma}^{\dagger} d_{\mathbf{k}, \nu', \sigma}, \quad (1)$$

resulting in a Fermi surface composed of three bands: a hole-like α band from quasi-1D orbitals and two electron-like β and γ bands, derived from quasi-1D and quasi-2D orbitals, respectively [2]. Here $\nu, \nu' \in \{xz, yz, xy\}$ index the t_{2g} orbitals, where $d_{\mathbf{k}, \nu, \sigma}^{\dagger}$ ($d_{\mathbf{k}, \nu, \sigma}$) is the fermionic creation (annihilation) operator for the orbital state ν with momentum \mathbf{k} and spin σ . Moreover, $\xi_{\nu}^{\mathbf{k}}$ represents the dispersion of orbital ν , $\mathcal{T}_{\nu, \nu'}^{\mathbf{k}}$ describes the hybridization between orbitals ν and ν' , and $\delta_{\nu, \nu'}$ is the Kronecker delta function. In contrast to the nearly k_z -independent d_{xy} orbital, the d_{xz} and d_{yz} orbitals exhibit significant k_z -dispersion, leading to orbital mixing that affects the β and γ bands at specific k_z values [44, 45]. Here, we focus on $k_z = \pi$, where the overlap between the d_{xy} and $d_{xz/yz}$ orbitals is maximized, and spin-orbit coupling effects are minimal [44]. The electronic dispersions at this k_z value, calculated via the tight-binding method, are given by

$$\begin{aligned} \xi_{xz}^{\mathbf{k}} &= -\mu - 2t_{xz}^x \cos k_x - 2t_{xz}^y \cos k_y, \\ \xi_{yz}^{\mathbf{k}} &= -\mu - 2t_{yz}^x \cos k_x - 2t_{yz}^y \cos k_y, \\ \xi_{xy}^{\mathbf{k}} &= -\mu - 2t_{xy}^x \cos k_x - 2t_{xy}^y \cos k_y - 4t_{xy}^{xy} \cos k_x \cos k_y, \\ \mathcal{T}_{xz, yz}^{\mathbf{k}} &= -4g \sin k_x \sin k_y, \quad \mathcal{T}_{xz, xy}^{\mathbf{k}} = -8g' \cos \frac{k_x}{2} \sin \frac{k_y}{2}, \\ \mathcal{T}_{yz, xy}^{\mathbf{k}} &= -8g' \cos \frac{k_y}{2} \sin \frac{k_x}{2}, \end{aligned} \quad (2)$$

where μ is the chemical potential, and $t_{\nu}^{x=y, xy}$ are the hopping parameters for orbital ν . The parameters g and g' characterize the intra-quasi-1D and inter-quasi-1D/2D orbital hopping strengths, respectively. The equilibrium tight-binding parameters are set to $(t_{xz}^x, t_{xz}^y, t_{xy}^x, t_{xy}^y, \mu, g, g') = (110, 7, 82, 37, 142, 9, 1)$ meV, and we consider $t_{yz}^x = t_{xz}^x$, $t_{yz}^y = t_{xz}^y$, and $t_{xy}^y = t_{xy}^x$ [33].

The chemical potential is crucial for applying biaxial strain. An increase in chemical potential causes van Hove singularities (vHS) in the [100] and [010] directions, leading to a Lifshitz transition. This also expands the γ sheet due to changes in orbital populations. While increasing the chemical potential indicates positive biaxial strain and the filling of the γ band, increasing g' moves the γ band away from the vHS near the Fermi level. These parameters influence the proximity of the β and γ sheets and the orbital weights from d_{xy} and $d_{xz/yz}$

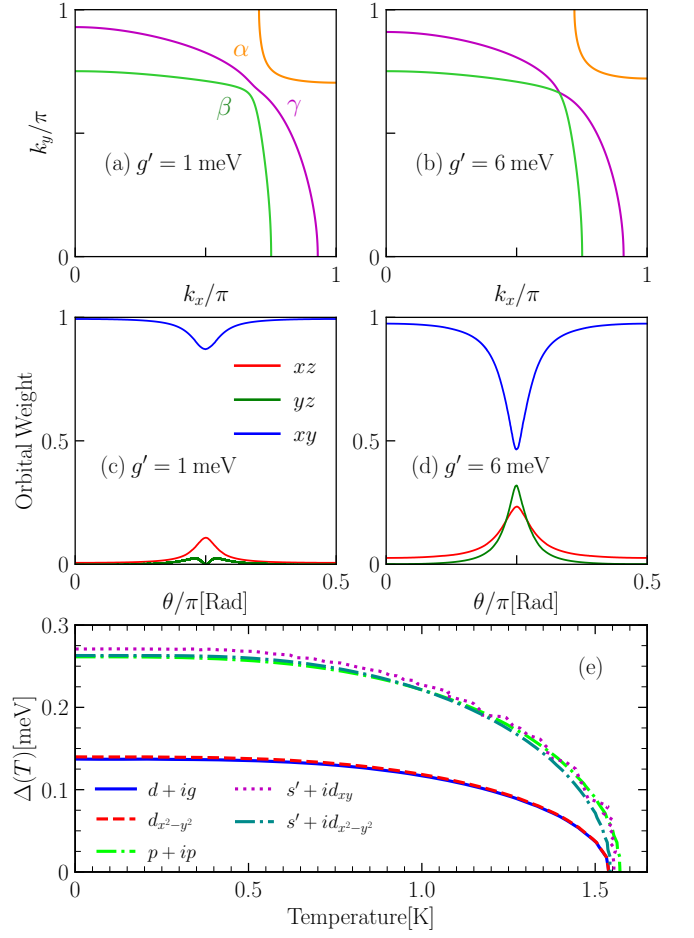


FIG. 1. Illustration of the effect of the parameter g' on the Fermi surface: (a) $g' = 1$ meV, and (b) $g' = 6$ meV, highlighting the touching of the two bands, β and γ , in the diagonal region, which predominantly contributes to the Berry curvature and Hall transport. (c) and (d) depict the variations in orbital weight on the γ -sheet along a quarter of the Brillouin zone for the respective values of g' , where $0 < \theta = \arctan(k_y/k_x) < \pi/2$. (e) Temperature dependence of the superconducting gap for different order parameters.

across the Fermi surface. Fig. 1(a) and Fig. 1(b) show that increasing g' significantly alters the diagonal region of Brillouin zone, causing the γ and β sheets to touch and increasing the separation between them and the hole-like α sheet. An increase in g' also brings about the reduction (increase) of the contribution of the d_{xy} quasi-2D orbital (d_{xz} and d_{yz} quasi-1D orbitals) to the γ sheet, see plots Fig. 1(c) and Fig. 1(d). The Hall response is influenced by the one-dimensional nature of the $d_{xz/yz}$ orbitals, making g' important for Hall transport. Specifically, higher g' leads to electron transfer from d_{xy} to $d_{xz/yz}$, decreasing the DOS near the Fermi level.

The multi-band structure leads to different superconducting gap textures [46], therefore, the superconducting Hamiltonian can be written as

$$\mathcal{H}_{SC} = \mathcal{H}_N + \sum_{\mathbf{k}\nu\nu'\sigma\sigma'} \left(\Delta_{\nu\nu'}^{\mathbf{k}} d_{-\mathbf{k}, \nu, \sigma}^{\dagger} d_{\mathbf{k}, \nu', \sigma'}^{\dagger} + \text{h.c.} \right), \quad (3)$$

Pairing	Momentum Dependence
(a) $d + ig$	$\Delta_{xy}^{\mathbf{k}} = [\Delta'_{xy}(T) + i\Delta''_{xy}(T) \sin k_x \sin k_y](\cos k_x - \cos k_y)$
(b) $d_{x^2-y^2}$	$\Delta_{xy}^{\mathbf{k}} = \Delta'_{xy}(T)(\cos k_x - \cos k_y)$
(c) $p + ip$	$\Delta_{xy}^{\mathbf{k}} = \Delta'_{xy}(T) \sin k_x + i\Delta''_{xy}(T) \sin k_y$
(d) $s' + id_{xy}$	$\Delta_{xy}^{\mathbf{k}} = \Delta'_{xy}(T)(\cos k_x + \cos k_y) + i\Delta''_{xy}(T) \sin k_x \sin k_y$
(e) $s' + id_{x^2-y^2}$	$\Delta_{xy}^{\mathbf{k}} = \Delta'_{xy}(T)(\cos k_x + \cos k_y) + i\Delta''_{xy}(T)(\cos k_x - \cos k_y)$

TABLE I. The most favored forms of the quasi-2D orbital superconducting order parameter, $\Delta_{xy}^{\mathbf{k}}$, for (a) $d + ig$: $d_{x^2-y^2} + ig_{xy(x^2-y^2)}$, (b) $d_{x^2-y^2}$, (c) $p + ip$: $p_x + ip_y$, (d) $s' + id_{xy}$, and (e) $s' + id_{x^2-y^2}$.

in which the elements of the superconducting order parameter are obtained through the solution of the self-consistency equation

$$\Delta_{\nu\nu'}^{\mathbf{k}} = -T \sum_{\omega_n} \sum_{\nu_1, \nu_1'} \sum_{\mathbf{k}'} g_{\nu\nu', \nu_1\nu_1'}^{\mathbf{k}, \mathbf{k}'} F_{\nu_1\nu_1'}(\mathbf{k}', \omega_n). \quad (4)$$

Here, $\omega_n = (2n+1)\pi T$ is the fermionic Matsubara frequency, and $F_{\nu\nu'}$ is the anomalous Green's function component. The superconducting coupling matrix $g_{\nu\nu', \nu_1\nu_1'}^{\mathbf{k}, \mathbf{k}'}$ defines the pairing interactions, and describes the orbital part of the coupling processes in momentum space. Specifically, this work focuses on the case of $g_{\nu\nu', \nu_1\nu_1'}^{\mathbf{k}, \mathbf{k}'} = g_{\nu\nu', \nu_1}^{\mathbf{k}, \mathbf{k}'}$, which indicates the intra-orbital pairing within a diagonal matrix format $\Delta_{\nu\nu'}^{\mathbf{k}} = \Delta_{\nu}^{\mathbf{k}}$. In this case, we can define the coupling matrix in a separable expression of

$$g_{\nu\nu_1}^{\mathbf{k}, \mathbf{k}'} = g'_{\nu\nu_1} f_{\nu}(\mathbf{k}) f_{\nu_1}'(\mathbf{k}') + g''_{\nu\nu_1} f_{\nu}''(\mathbf{k}) f_{\nu_1}''(\mathbf{k}'), \quad (5)$$

with form factors $f_{\nu}(\mathbf{k}) = f_{\nu}(\mathbf{k}) + if_{\nu}''(\mathbf{k})$ for the orbital ν , encoding the momentum dependence of the interaction [47–50]. It represents intra-orbital Cooper pairs, where pairing occurs within the same orbital ($\nu = \nu_1$) or involves hopping to a different orbitals ($\nu \neq \nu_1$) [51]. For Sr_2RuO_4 with a two-dimensional square lattice, the gap symmetry can be classified based on the irreducible representations (irrep) of the D_{4h} group, namely extended s -wave (s'), $d_{x^2-y^2}$, d_{xy} , $g_{xy(x^2-y^2)}$, and $p_x(p_y)$. We focus on a time reversal symmetry breaking phase with chiral character for the quasi-1D orbitals, which belong to the E_u irrep of the D_{4h} point group. Thus, the superconducting order parameter can be expressed as $\Delta_{\nu\nu'}^{\mathbf{k}} = \Delta_{\nu}^{\mathbf{k}} = \Delta'_{\nu}(T) f_{\nu}(\mathbf{k}) + i\Delta''_{\nu}(T) f_{\nu}''(\mathbf{k})$. Correspondingly, for $\Delta_{xz}^{\mathbf{k}}$ and $\Delta_{yz}^{\mathbf{k}}$, we can consider $(f_{xz}'(\mathbf{k}), f_{xz}''(\mathbf{k}), f_{yz}'(\mathbf{k}), f_{yz}''(\mathbf{k})) = (\sin k_x, 0, 0, \sin k_y)$ with $\Delta_{xz}'(T) = \Delta_{yz}'(T)$ [36, 38], however, for $\Delta_{xy}^{\mathbf{k}}$, we analyze the preferred forms of the orbital order parameter presented in Table I [8, 9, 52–54].

Fig. 1(e) shows the BCS prediction for the temperature-dependent order parameter in the d_{xy} orbital, $\Delta_{xy}(T)$, across the considered forms. The focus here is on the d_{xy} orbital, as variations in the coupling g' and chemical potential impact its DOS near the Fermi level. We determine the magnitude of Δ_0 , by adjusting the pairing strengths in the channels listed in Table I to yield a transition temperature in line with experimental values, $T_c = 1.5\text{K}$ [1]. The calculated values for the $p + ip$, $s' + id_{xy}$, and $s' + id_{x^2-y^2}$ pairings are nearly identical at $\Delta_0 = 0.26\text{meV}$, while for the $d + ig$ and $d_{x^2-y^2}$ pairings, Δ_0 is found to be 0.14meV . To facilitate comparison between different pairing states, we examine the effect of g'

and μ on the critical temperature T_c . This analysis helps narrow down possible pairing channels and identify the favored pairing for the d_{xy} orbital. The results show a pronounced sensitivity of T_c to increases in g' and μ across various pairings. For the $d + ig$ and $d_{x^2-y^2}$ pairings, T_c reaches a significant peak, more than doubling, as it approaches the critical chemical potential, $\mu_c = 148\text{meV}$. This critical point corresponds to a Lifshitz transition, characterized by a Fermi surface reconstruction where the vHS intersect the Fermi level at points $(k_x, k_y) = (0, \pm\pi)$ and $(\pm\pi, 0)$ within the Brillouin zone. Beyond μ_c , T_c declines rapidly as a function of the particle concentration in the d_{xy} orbital. In contrast, for the $p + ip$, $s' + id_{xy}$, and $s' + id_{x^2-y^2}$ pairings, T_c shows minimal sensitivity to the vHS, with no peak near μ_c . This difference arises because the gap functions of $p + ip$ and $s' + id_{xy}$ vanish at the vHS points, while the $s' + id_{x^2-y^2}$ pairing has a purely imaginary gap function at these points. By comparison, the favored pairings, $d + ig$ and $d_{x^2-y^2}$, retain real-valued gap functions at the vHS points. The influence of the coupling parameter g' on T_c is consistent across the $d + ig$, $d_{x^2-y^2}$, and $p + ip$ pairings, where increasing g' results in a decrease in T_c . This decrease is attributed to g' shifting the peak of the d_{xy} orbital DOS away from the Fermi level. This behavior is in direct contrast to the effect of μ , which generally enhances T_c by moving the DOS peak closer to the Fermi level.

III. OPTICAL HALL CONDUCTIVITY

Reformulating the superconducting Hamiltonian with a 6×6 matrix to account for the 2 Nambu and 3 orbital degrees of freedom, the bare Green's function in the superconducting state is given by

$$\hat{G}_0(\mathbf{k}, iv_n) = \begin{bmatrix} \hat{G}_0(\mathbf{k}, iv_n) & \hat{F}_0(\mathbf{k}, iv_n) \\ \hat{F}_0^\dagger(\mathbf{k}, iv_n) & -\hat{G}_0^T(-\mathbf{k}, -iv_n) \end{bmatrix}, \quad (6)$$

in which $\hat{G}_0(\mathbf{k}, i\omega_m)$ and $\hat{F}_0(\mathbf{k}, i\omega_m)$ are the normal and anomalous Green's functions, respectively. Within the linear response theory, the dynamical Hall conductivity is given by the following Kubo formula

$$\sigma^H(\omega) = \frac{1}{2} \lim_{\mathbf{q} \rightarrow 0} [\sigma_{x,y}(\mathbf{q}, \omega) - \sigma_{y,x}(\mathbf{q}, \omega)], \quad (7)$$

where

$$\sigma_{i,j}(\mathbf{q}, \omega) = \frac{i}{\omega} K_{i,j}(\mathbf{q}, \omega); \quad i, j \in \{x, y\},$$

and $K_{i,j}(\mathbf{q}, \omega)$ is the current-current correlation function that is obtained from the analytical continuation, $i\omega_m \rightarrow \omega + i0^+$, of its Matsubara counterpart

$$K_{i,j}(\mathbf{q}, i\omega_m) = T \sum_{\mathbf{k}, i\nu_n} \text{Tr} \left[\hat{\mathcal{J}}_i(\mathbf{k}) \hat{\mathcal{G}}_0(\mathbf{k}, i\nu_n) \hat{\mathcal{J}}_j(\mathbf{k}) \hat{\mathcal{G}}_0(\mathbf{k} + \mathbf{q}, i\nu_n + i\omega_m) \right]. \quad (8)$$

Here, $\hat{\mathcal{J}}(\mathbf{k})$ is the charge current operator represented as a 6×6 -rank tensor, and $\nu_n = (2n + 1)\pi T$ and $\omega_m = 2m\pi T$ are the Matsubara fermionic and bosonic frequencies, respectively. After performing straightforward calculations [38], the final expression for the dynamical Hall conductivity can be expressed as

$$\sigma^H(\omega) = \frac{e^2}{\hbar} \sum_{\mathbf{k}} \sum_{\substack{\nu, \nu', \nu'' \\ (\nu \neq \nu' \neq \nu'')}} \mathcal{T}_{\nu, \nu'}^{\mathbf{k}}, \text{Im}[\Delta_{\nu}^{\mathbf{k}} \Delta_{\nu'}^{\mathbf{k}*}] \times [v_{x\nu\nu'}^{\mathbf{k}}(v_{y\nu'}^{\mathbf{k}} - v_{y\nu}^{\mathbf{k}}) - v_{y\nu\nu'}^{\mathbf{k}}(v_{x\nu}^{\mathbf{k}} - v_{x\nu'}^{\mathbf{k}})] \Upsilon_{\nu''}(\mathbf{k}, i\omega), \quad (9)$$

where

$$\Upsilon_{\nu}(\mathbf{k}, i\omega) = \sum_z \frac{(z - z')(z + z')^2 [z^2 - E_{\nu}(\mathbf{k})^2] [z'^2 - E_{\nu}(\mathbf{k})^2]}{\prod_{i=1,2,3} [z^2 - E_i(\mathbf{k})^2] [z'^2 - E_i(\mathbf{k})^2]}, \quad (10)$$

in which $z = i\nu_n$ and $z' = z + i\omega_m$. Here, $v_{l\nu\nu'}^{\mathbf{k}} = \partial \mathcal{T}_{\nu, \nu'}^{\mathbf{k}} / \partial k_l$ and $v_{l\nu}^{\mathbf{k}} = \partial \xi_{\nu}^{\mathbf{k}} / \partial k_l$ ($l = x, y$) are interorbital velocity and intraorbital velocity, respectively, and in fact are the elements of the 3×3 bare current vertex in the orbital basis. Furthermore, $E_{\nu}(\mathbf{k}) = \sqrt{\xi_{\nu}^{\mathbf{k}^2} + \Delta_{\nu}^{\mathbf{k}^2}}$, and the BCS quasiparticle spectra $E_i(\mathbf{k})$ are obtained via the relation

$$\det \hat{\mathcal{G}}_0^{-1}(\mathbf{k}, z) \propto \prod_{i=1,2,3} [z^2 - E_i(\mathbf{k})^2].$$

After carrying out the Matsubara summation in the expression of Eq. (10), it becomes

$$\begin{aligned} \Upsilon_{\nu}(\mathbf{k}, i\omega) = & \frac{E_{\nu}(\mathbf{k})^4 - E_{\nu}(\mathbf{k})^2 [E_1(\mathbf{k})^2 + E_2(\mathbf{k})^2] + [E_1(\mathbf{k})E_2(\mathbf{k})]^2}{E_1(\mathbf{k})E_2(\mathbf{k})[E_2(\mathbf{k})^2 - E_3(\mathbf{k})^2][E_3(\mathbf{k})^2 - E_1(\mathbf{k})^2]} \times \\ & \left[\frac{f(E_1(\mathbf{k})) - f(E_2(\mathbf{k}))}{[E_1(\mathbf{k}) - E_2(\mathbf{k})]([E_1(\mathbf{k}) - E_2(\mathbf{k})]^2 - (i\omega)^2)} \right. \\ & \left. + \frac{1 - f(E_1(\mathbf{k})) - f(E_2(\mathbf{k}))}{[E_1(\mathbf{k}) + E_2(\mathbf{k})]([E_1(\mathbf{k}) + E_2(\mathbf{k})]^2 - (i\omega)^2)} \right] \\ & + (1 \rightarrow 2 \text{ and } 2 \rightarrow 3) + (1 \rightarrow 3 \text{ and } 2 \rightarrow 1), \end{aligned} \quad (11)$$

where $f(E_{\nu}(\mathbf{k}))$ refers to the finite-temperature Fermi-Dirac function.

Eq. (9) states that to have Hall-type response, at least one of the orbital gap functions must be complex. The chiral character rises due to the multiple order parameter of the quasi-1D

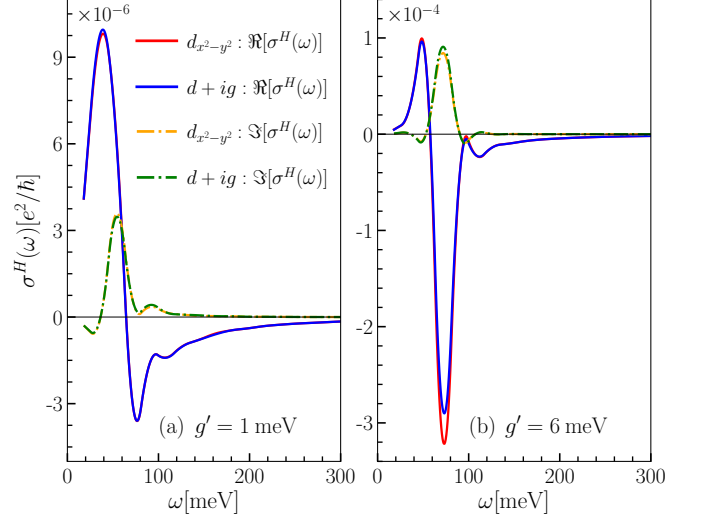


FIG. 2. The comparison between the dynamical Hall conductivity, $\sigma^H(\omega)$, for the pairing channels $d + ig$ and $d_{x^2-y^2}$ that indicates the role of the breaking of the time reversal symmetry on the gap function of the orbital d_{xy} with (a) $g' = 1 \text{ meV}$, and (b) $g' = 6 \text{ meV}$.

orbitals, and we set the gap functions $d + ig$ and $d_{x^2-y^2}$ on the orbital d_{xy} . The other requirement which must be met, is \mathbf{k} -dependent inter-orbital coupling. In Fig. 2, the dynamical Hall conductivity is shown for the favored pairings, $d + ig$ and $d_{x^2-y^2}$, at two different coupling values, $g' = 1 \text{ meV}$ and $g' = 6 \text{ meV}$. From this, two main conclusions arise: First, the coupling parameter g' significantly influences the Hall conductivity. This effect is likely due to changes in the convex and concave portions of the Fermi surfaces, which contribute positively and negatively to the Hall conductivity, respectively [55]. Secondly, the Hall response is found to be identical for both pairings, which indicates that the time-reversal symmetry breaking in the gap function of the d_{xy} orbital does not affect the Hall-type response in this context. The main contribution to the dynamical Hall conductivity arises from the term involving $\mathcal{T}_{xz,yz}^{\mathbf{k}}$. Thus, in the following, we consider pairing $d_{x^2-y^2}$ for the d_{xy} orbital and focus on the term with inter-orbital coupling $\mathcal{T}_{xz,yz}^{\mathbf{k}}$. We observe that the dominant contribution to the Hall-type response originates from the quasiparticle energy spectra $E_1(\mathbf{k})$ and $E_2(\mathbf{k})$, whereas the spectrum $E_3(\mathbf{k})$, which is closest to the Fermi level, contributes negligibly.

A peak or resonance in the response function appears due to the coherence factor, which maintains a high density of states. Therefore, considering peaks in both quantities is an essential step forward [56]. Fig. 3 shows the DOS in the superconducting state, with the $p + ip$ wave on the quasi-1D orbitals and the $d + ig$ pairing on the quasi-2D orbital, at zero temperature across different values of coupling g' and μ . At low energies, the DOS develops three main coherence peaks at $\omega \simeq \Delta_0$, $\omega \simeq 2\Delta_0$, and $\omega \simeq 8g'$. The influence of interorbital coupling g' causes significant changes in the DOS: an increase in g' increases the intensity of the second peak and shifts the third peak to higher energies. As the chemical potential μ

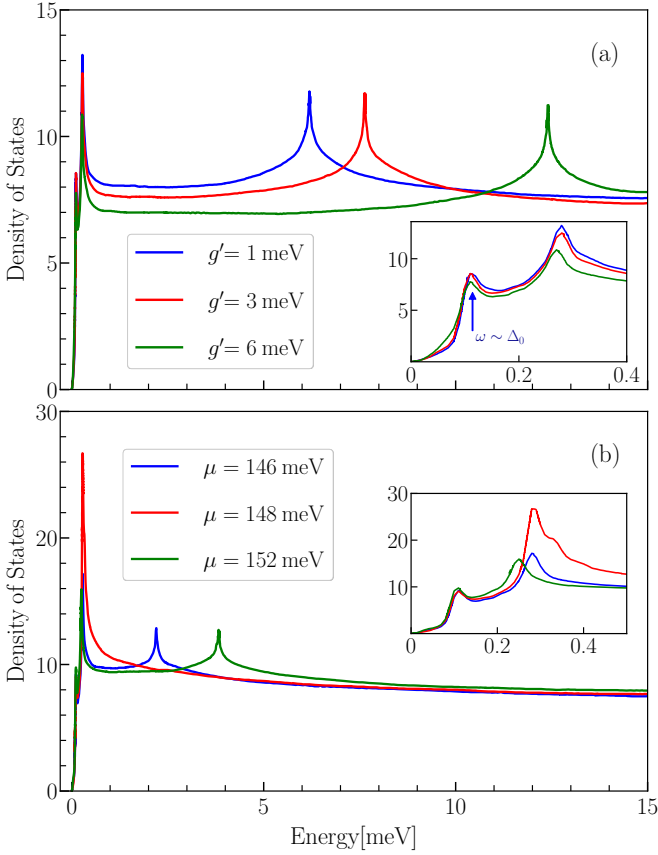


FIG. 3. The DOS in the superconducting state is shown for the $p+ip$ wave pairing on the quasi-1D orbitals and the $d+ig$ wave pairing on the quasi-2D orbital at $T = 0$: (a) for different g' values with $\mu = 142$ meV, and (b) for different μ values with $g' = 1$ meV. The insets show the same data with a zoomed-in view for the low-energy regimes.

increases, the first and second peaks are enhanced, and the third peak shifts to lower energies. At the critical chemical potential $\mu = \mu_c$, the third peak merges with the second peak. This critical point marks the crossing of van Hove singularities with the Fermi level, resulting in an increased DOS at low energies and the elimination of the second peak. With a further increase in μ , the third peak reappears at lower energies, corresponding to the hole-like Fermi surface. Notably, a fourth peak appears at higher energies, specifically at $\omega \simeq 4g$, which drives the primary resonance in the Hall-type response (see Fig. 2). This peak remains unaffected by variations in g' and μ , and is therefore omitted from the present figure.

The behavior of the coherence factor in the $\sigma^H(\omega)$, i.e. the coefficient of function $\Upsilon_\nu(\mathbf{k}, i\omega)$ multiplied by function $\mathcal{T}_{\nu,\nu'}^{\mathbf{k}}, \text{Im}[\Delta_\nu^{\mathbf{k}} \Delta_{\nu'}^{\mathbf{k}*}]$ [32], is influenced by the proximity (touching) conditions between multiple Fermi surface sheets, which in turn control the peak positions in the response function. This proximity is predominantly occurred in the diagonal regions ([110] and [1 $\bar{1}$ 0]) rather than in the [100] and [010] directions, resulting in a significant reduction of the coherence factors along the k_x and k_y axes. In the absence of impurities the multi-orbital nature of the system primarily contributes to

the observed Hall response.

IV. POLAR KERR EFFECT

Using the standard formalism for Kerr rotation and incorporating the dynamical Hall conductivity, the polar Kerr angle can be evaluated as [30]

$$\theta^{Kerr}(\omega) = \frac{4\pi}{\omega d} \text{Im} \left[\sigma^H(\omega) \varphi(\omega) \right], \quad (12)$$

where $1/\varphi(\omega) = n(\omega)[n(\omega)^2 - 1]$, and $n(\omega) = \sqrt{\epsilon_\infty + (4\pi i/\omega)\sigma(\omega)}$ denotes the refraction index. Here $\epsilon_\infty = 10$ refers to the background dielectric tensor, and $d = 6.8\text{\AA}$ is the interlayer distance. Obviously, the refraction index is defined by the complex longitudinal optical conductivity $\sigma(\omega)$. For simplicity, without any loss of generality, the calculation can be performed using a two-orbital model [57]. In which, the first orbital represents the sum of quasi-1D orbitals, denoted as $d_{xz} + d_{yz}$, while the second orbital corresponds to the quasi-2D orbital d_{xy} . This model arises due to the tetragonal symmetry of Sr_2RuO_4 and the distinct orbital characteristics of the three Fermi surfaces. These features suggest that the dominant pairing channel originates from either the quasi-2D orbital d_{xy} or the quasi-1D orbitals $d_{xz/yz}$ [58]. Following Refs. [59], the conductivity is obtained by solving two coupled equations of motion for free charges, characterized by the velocities \mathbf{V}_κ and \mathbf{V}_ι in the orbitals κ and ι , respectively. This leads to the expression

$$\begin{aligned} -i\omega m_\iota \mathbf{V}_\iota &= -\frac{m_\iota \mathbf{V}_\iota}{\tau_\iota} + q_\iota \mathbf{E} - \mathbf{g}_{ee} n_\kappa (\mathbf{V}_\iota - \mathbf{V}_\kappa), \\ -i\omega m_\kappa \mathbf{V}_\kappa &= -\frac{m_\kappa \mathbf{V}_\kappa}{\tau_\kappa} + q_\kappa \mathbf{E} - \mathbf{g}_{ee} n_\iota (\mathbf{V}_\kappa - \mathbf{V}_\iota), \end{aligned} \quad (13)$$

where $m_{\iota(\kappa)}$, $q_{\iota(\kappa)}$, $n_{\iota(\kappa)}$, and $\tau_{\iota(\kappa)}$ denote the effective mass, charge, particle density, and scattering time of the charge carriers in the orbital $\iota(\kappa)$, respectively. Moreover, \mathbf{E} denotes the electric field, and \mathbf{g}_{ee} represents the interorbital electron-electron scattering, which becomes relevant only at non-zero temperatures. We continue by calculating the velocities $\mathbf{V}_\iota(\kappa)$, which is given by

$$\mathbf{V}_\iota(\kappa) = \frac{m_{\kappa(\iota)} q_{\iota(\kappa)} (\tau_{\kappa(\iota)}^{-1} - i\omega) + \mathbf{g}_{ee} (n_\iota q_\iota + n_\kappa q_\kappa)}{m_\iota m_\kappa \left((\gamma_0^2 - \omega^2) - \frac{i\omega}{\tau'} \right)} \mathbf{E}, \quad (14)$$

with

$$\begin{aligned} \frac{1}{\tau'} &= \frac{1}{\tau_\iota} + \frac{1}{\tau_\kappa} + \frac{1}{\tau}, \\ \gamma_0^2 &= \frac{1}{\tau_\iota \tau_\kappa} + \frac{1}{\tau} \left[\frac{1}{\tau_\iota \left(1 + \frac{n_\kappa m_\kappa}{n_\iota m_\iota} \right)} + \frac{1}{\tau_\kappa \left(1 + \frac{n_\iota m_\iota}{n_\kappa m_\kappa} \right)} \right], \\ \frac{1}{\tau} &= \mathbf{g}_{ee} \left(\frac{n_\iota}{m_\kappa} + \frac{n_\kappa}{m_\iota} \right), \end{aligned} \quad (15)$$

After performing some calculations and comparing the relations for the current $\mathbf{J} = n_\iota q_\iota \mathbf{V}_\iota + n_\kappa q_\kappa \mathbf{V}_\kappa$ and $\mathbf{J} = \sigma(\omega) \mathbf{E}$,

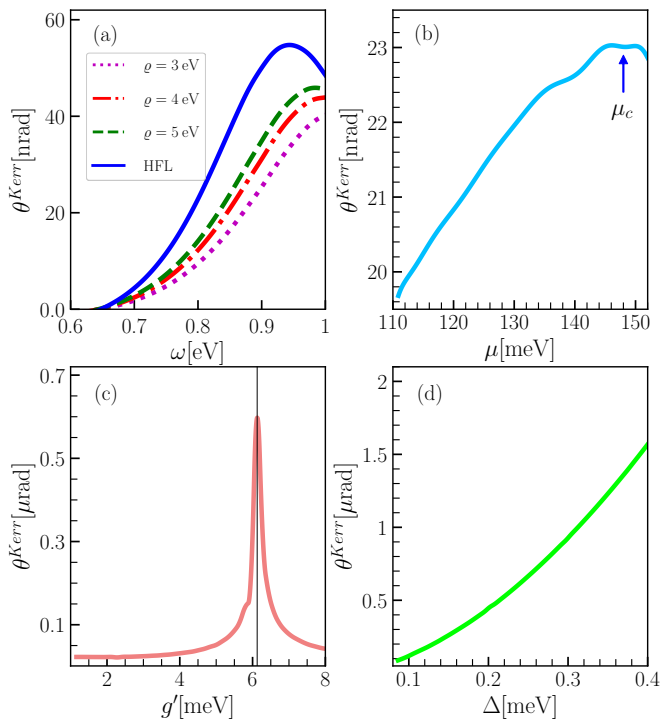


FIG. 4. a) Kerr rotation angle (in unit of nanoradian) versus photon energy. The non-solid curves represent the influence of the interband electron-electron scattering on the Kerr angle in the hydrodynamic regime, $\rho = 1/\tau \gg 1/\tau_l \sim 1/\tau_\kappa$. The blue solid curve indicates the Kerr signal in the high frequencies limit (HFL), where the longitudinal conductivity is described by the Drude formula. The Kerr polar angle is shown: (b) as a function of the chemical potential μ with $g' = 1$ meV and $\Delta = 0.14$ meV, (c) as a function of the interorbital coupling or z -direction hopping g' with $\mu = 142$ meV and $\Delta = 0.14$ meV, we plotted it in the possible range from 0 to 8 meV [60], and (d) as a function of the gap function magnitude Δ with $g' = 1$ meV and $\mu = 142$ meV. We set $\omega = 0.8$ eV [26], although the general behavior remains consistent across other frequency ranges. The maximum signal corresponds to the formation of near-Fermi-energy degenerate states between the β and γ bands. The region near the maximum in plot (c) corresponds to specific z -direction hopping values that induce a concave curvature in the Fermi surface of the γ sheet.

we obtain the conductivity $\sigma(\omega)$ as

$$\sigma(\omega) = \frac{1}{4\pi} \frac{\frac{\omega_{lp}^2}{\tau_\kappa} + \frac{\omega_{\kappa p}^2}{\tau_l} + \frac{\omega_0^2}{\tau} - i\omega\omega_p^2}{(\gamma_0^2 - \omega^2) - \frac{i\omega}{\tau}}, \quad (16)$$

where $\omega_{lp}^2 = (n_l q_l^2)/m_l$ is the plasma frequency of the orbital l , $\omega_p^2 = \omega_{lp}^2 + \omega_{\kappa p}^2$ and $\omega_0^2 = 4\pi(n_l q_l + n_\kappa q_\kappa)^2/(n_l m_l + n_\kappa m_\kappa)$. Note that τ only depends on the temperature not frequency.

Considering a generic case, when $n_l \sim n_\kappa$ and $m_l \sim m_\kappa$ which implies that $\omega_{lp} \sim \omega_{\kappa p} \sim \omega_p \sim \omega_0 = 2.9$ eV and $\tau_l^{-1} \sim \tau_\kappa^{-1} = 0.4$ eV [59], one can focus on two regimes: (i) the high-frequency limit, where the longitudinal conductivity is described by the Drude formula, and (ii) the hydrodynamic regime, characterized by the condition

$\rho = \tau^{-1} \gg \tau_l^{-1} \sim \tau_\kappa^{-1}$ [59]. In this context, Fig. 4(a) presents the Kerr rotation angle (in units of nanoradians) as a function of photon energy. The blue-solid curve represents the Kerr signal in the high-frequency limit. The remaining curves correspond to e - e scattering for $\rho = 3, 4,$ and 5 eV, which are relevant in the hydrodynamic regime and highlight the effect of interband electron-electron scattering on the Kerr angle. We observe that while scattering enhances the Kerr polar angle, the enhancement remains smaller than that observed in the high-frequency limit. Moreover, we plot the Kerr polar angle as a function of the chemical potential in the Fig. 4(b), the z -direction hopping in the Fig. 4(c), and the pairing amplitude in the Fig. 4(d), all at the frequency $\omega = 0.8$ eV [30]. Fig. 4(b) demonstrates that as the chemical potential increases, $\theta^{Kerr}(\omega)$ rises until it crosses the van Hove point $\mu = \mu_c$, where a Lifshitz transition occurs. After this point, the superconducting character of the γ band becomes fragile. As seen in Fig. 4(c), increasing the coupling g' leads to an increase in the Kerr angle. This is expected, as increasing g' is equivalent to transferring an electron from the 2D quasi-orbital to the 1D quasi-orbitals, and it is anticipated that this transfer will result in an increase in the Kerr angle. A sharp peak in the Kerr angle is observed at $g' \simeq 6$ meV, where the touching between the bands β and γ is largest and the nearly degenerate low-energy electronic states are formed, i.e., the change in band dispersion in vicinity of the Fermi energy. In fact, the region around the peak, is related to the appearance of the concavity on the band γ . Fig. 4(d) illustrates the dependence of the Kerr angle on the pairing amplitude, highlighting the role of temperature in the Kerr angle. As temperature increases, the amplitude of the gap function decreases, which in turn reduces the Kerr angle.

At the end, we should emphasize that the real part of the dynamical Hall conductivity follows a similar trend to the Kerr polar angle. This similarity is based on the fact that the imaginary part of the Hall-type response vanishes at high frequencies, as shown in the Fig. 2.

V. CONCLUSION

We have investigated the Hall-type response of the superconductor Sr_2RuO_4 in two physical scenarios. The first scenario involves inducing a Lifshitz transition in the largest Fermi surface sheet, causing it to reshape from an electron-like to a hole-like (open sheet) configuration as the chemical potential, μ , is increased. The second scenario explores the impact of retracting the previously mentioned sheet from the van Hove points by adjusting the coupling between the quasi-1D and quasi-2D orbitals, i.e., the z -direction hopping parameter g' . Initially, we found $d + ig$ and $d_{x^2-y^2}$ pairing channels as the leading candidates for the d_{xy} orbital in the weak-coupling limit. These two channels exhibit the correct and expected behaviors as μ and g' vary such that tuning the chemical potential μ leads to increasing the superconducting transition temperature whereas g' results in a reverse effect. Using a self-consistent approach, we have determined

the magnitude of these pairings at the zero-temperature limit around $\Delta_0 = 0.14\text{meV}$. Furthermore, we have discovered that the optical response for these two pairings are identical. This finding suggests that the time-reversal symmetry breaking of the gap function in the d_{xy} orbital is not required to produce a finite Kerr angle.

Similar to the two-orbital model, the primary peak in the response function arises in vicinity of the coupling amplitude between the quasi-1D orbitals. Increasing g' affects the frequency region around this peak, leading to negative conductivity, similar to the effect of increasing μ . These effects are examined using the coherence factor. We have found that g' shifts the superconducting DOS peak to higher energies, while μ pushes it to lower energy levels. Finally, we have studied the effects of electron-electron scattering, the gap function amplitude (or equivalently temperature), g' , and μ on the Kerr angle. The effect of the former case is an enhancement of the Kerr

signal in the high-frequency limit. As expected, the Kerr angle increases with the gap amplitude. Additionally, the key effect of g' occurs around $\sim 6\text{meV}$, where a sharp peak emerges, corresponding to the increase in the orbital weight of quasi-1D orbitals. This is accompanied by the formation of near-Fermi energy degenerate states between the β and γ bands, resulting from the enhanced dispersive state of the γ band near the Fermi level. Moreover, the chemical potential, μ , enhances the Kerr angle until it reached its critical value. In conclusion, the Hall response can be tuned by adjusting various parameters, such as transferring electrons to the quasi-1D orbitals and enhancing superconductivity with increasing chemical potential, provided that the system does not undergo a Lifshitz transition that leads to an open geometry. Additionally, these two parameters significantly influence the superconducting transition temperature by modifying the proximity of the Fermi surfaces associated with the β and γ bands.

-
- [1] Y. Maeno, H. Hashimoto, K. Yoshida, S. Nishizaki, T. Fujita, J. G. Bednorz, and F. Lichtenberg, Superconductivity in a layered perovskite without copper, *Nature* **372**, 532 (1994).
- [2] A. P. Mackenzie and Y. Maeno, The superconductivity of Sr_2RuO_4 and the physics of spin-triplet pairing, *Rev. Mod. Phys.* **75**, 657 (2003).
- [3] M. E. Barber, A. Steppke, A. P. Mackenzie, and C. W. Hicks, Piezoelectric-based uniaxial pressure cell with integrated force and displacement sensors, *Review of Scientific Instruments* **90**, 023904 (2019).
- [4] F. Jerzembeck, H. S. Røising, A. Steppke, H. Rosner, D. A. Sokolov, N. Kikugawa, T. Scaffidi, S. H. Simon, A. P. Mackenzie, and C. W. Hicks, The superconductivity of Sr_2RuO_4 under c-axis uniaxial stress, *Nature Communications* **13**, 4596 (2022).
- [5] C. W. Hicks, F. Jerzembeck, H. M. Noad, M. E. Barber, and A. P. Mackenzie, Probing quantum materials with uniaxial stress, *Annual Review of Condensed Matter Physics* <https://doi.org/10.1146/annurev-conmatphys-040521-041041> (2024).
- [6] A. P. Mackenzie, T. Scaffidi, C. W. Hicks, and Y. Maeno, Even odder after twenty-three years: the superconducting order parameter puzzle of Sr_2RuO_4 , *npj Quantum Materials* **2**, 40 (2017).
- [7] Y. Maeno, A. Ikeda, and G. Mattoni, Thirty years of puzzling superconductivity in Sr_2RuO_4 , *Nature Physics* **20**, 1712 (2024).
- [8] C. W. Hicks, D. O. Brodsky, E. A. Yelland, A. S. Gibbs, J. A. N. Bruin, M. E. Barber, S. D. Edkins, K. Nishimura, S. Yonezawa, Y. Maeno, and A. P. Mackenzie, Strong increase of T_c of Sr_2RuO_4 under both tensile and compressive strain, *Science* **344**, 283 (2014).
- [9] A. Steppke, L. Zhao, M. E. Barber, T. Scaffidi, F. Jerzembeck, H. Rosner, A. S. Gibbs, Y. Maeno, S. H. Simon, A. P. Mackenzie, and C. W. Hicks, Strong peak in T_c of Sr_2RuO_4 under uniaxial pressure, *Science* **355**, eaaf9398 (2017).
- [10] F. Jerzembeck, Y.-S. Li, G. Palle, Z. Hu, M. Biderang, N. Kikugawa, D. A. Sokolov, S. Ghosh, B. J. Ramshaw, T. Scaffidi, M. Nicklas, J. Schmalian, A. P. Mackenzie, and C. W. Hicks, T_c and the elastocaloric effect of Sr_2RuO_4 under $\langle 110 \rangle$ uniaxial stress: No indications of transition splitting, *Phys. Rev. B* **110**, 064514 (2024).
- [11] S. Cobo, F. Ahn, I. Eremin, and A. Akbari, Anisotropic spin fluctuations in Sr_2RuO_4 : Role of spin-orbit coupling and induced strain, *Phys. Rev. B* **94**, 224507 (2016).
- [12] A. Pustogow, Y. Luo, A. Chronister, Y.-S. Su, D. Sokolov, F. Jerzembeck, A. P. Mackenzie, C. W. Hicks, N. Kikugawa, S. Raghu, *et al.*, Constraints on the superconducting order parameter in Sr_2RuO_4 from oxygen-17 nuclear magnetic resonance, *Nature* **574**, 72 (2019).
- [13] Y. Luo, A. Pustogow, P. Guzman, A. P. Dioguardi, S. M. Thomas, F. Ronning, N. Kikugawa, D. A. Sokolov, F. Jerzembeck, A. P. Mackenzie, C. W. Hicks, E. D. Bauer, I. I. Mazin, and S. E. Brown, Normal state ^{17}O nmr studies of Sr_2RuO_4 under uniaxial stress, *Phys. Rev. X* **9**, 021044 (2019).
- [14] A. T. Rømer, A. Kreisel, M. A. Müller, P. J. Hirschfeld, I. M. Eremin, and B. M. Andersen, Theory of strain-induced magnetic order and splitting of T_c and T_{TRSB} in Sr_2RuO_4 , *Phys. Rev. B* **102**, 054506 (2020).
- [15] A. Chronister, M. Zingl, A. Pustogow, Y. Luo, D. Sokolov, F. Jerzembeck, N. Kikugawa, C. Hicks, J. Mravlje, E. Bauer, *et al.*, Tuning the fermi liquid crossover in Sr_2RuO_4 with uniaxial stress, *npj Quantum Materials* **7**, 113 (2022).
- [16] F. Jerzembeck, A. Steppke, A. Pustogow, Y. Luo, A. Chronister, D. A. Sokolov, N. Kikugawa, Y.-S. Li, M. Nicklas, S. E. Brown, A. P. Mackenzie, and C. W. Hicks, Upper critical field of Sr_2RuO_4 under in-plane uniaxial pressure, *Phys. Rev. B* **107**, 064509 (2023).
- [17] C. W. Hicks, M. E. Barber, S. D. Edkins, D. O. Brodsky, and A. P. Mackenzie, Piezoelectric-based apparatus for strain tuning, *Review of Scientific Instruments* **85**, 065003 (2014).
- [18] R. Matzdorf, Z. Fang, null, J. Zhang, T. Kimura, Y. Tokura, K. Terakura, and E. W. Plummer, Ferromagnetism stabilized by lattice distortion at the surface of the p_x -Wave superconductor Sr_2RuO_4 , *Science* **289**, 746 (2000).
- [19] C. N. Veenstra, Z.-H. Zhu, B. Ludbrook, M. Capsoni, G. Levy, A. Nicolaou, J. A. Rosen, R. Comin, S. Kittaka, Y. Maeno, I. S. Elfimov, and A. Damascelli, Determining the surface-to-bulk progression in the normal-state electronic structure of Sr_2RuO_4 by angle-resolved photoemission and density functional theory, *Phys. Rev. Lett.* **110**, 097004 (2013).
- [20] Y. Imai, K. Wakabayashi, and M. Sigrist, Effect of Lifshitz transition on thermal transport properties in Sr_2RuO_4 , *Physics Pro-*

- cedia **75**, 150 (2015), 20th International Conference on Magnetism, ICM 2015.
- [21] K. M. Shen, N. Kikugawa, C. Bergemann, L. Balicas, F. Baumberger, W. Meevasana, N. J. C. Ingle, Y. Maeno, Z.-X. Shen, and A. P. Mackenzie, Evolution of the fermi surface and quasiparticle renormalization through a van hove singularity in $\text{Sr}_{2-y}\text{La}_y\text{RuO}_4$, *Phys. Rev. Lett.* **99**, 187001 (2007).
- [22] R. Nishinakayama, Y. J. Sato, T. Yamanaka, Y. Maeno, H. Yaguchi, N. Kikugawa, and R. Okazaki, Negatively enhanced thermopower near a van hove singularity in electron-doped Sr_2RuO_4 , *Phys. Rev. Res.* **6**, 023222 (2024).
- [23] B. Kim, S. Khmelevskiy, C. Franchini, I. I. Mazin, and K. Kim, SrRuO_3 - SrTiO_3 heterostructure as a possible platform for studying unconventional superconductivity in Sr_2RuO_4 , *Phys. Rev. B* **101**, 220502 (2020).
- [24] C. Kallin, Chiral p-wave order in Sr_2RuO_4 , *Reports on Progress in Physics* **75**, 042501 (2012).
- [25] Y. Maeno, S. Kittaka, T. Nomura, S. Yonezawa, and K. Ishida, Evaluation of spin-triplet superconductivity in Sr_2RuO_4 , *Journal of the Physical Society of Japan* **81**, 011009 (2012).
- [26] J. Xia, Y. Maeno, P. T. Beyersdorf, M. M. Fejer, and A. Kapitulnik, High resolution polar kerr effect measurements of Sr_2RuO_4 : Evidence for broken time-reversal symmetry in the superconducting state, *Phys. Rev. Lett.* **97**, 167002 (2006).
- [27] W. Kim, F. Marsiglio, and C. S. Ting, Hall conductivity of a spin-triplet superconductor, *Phys. Rev. Lett.* **100**, 227003 (2008).
- [28] J. Goryo, Impurity-induced polar kerr effect in a chiral p-wave superconductor, *Phys. Rev. B* **78**, 060501 (2008).
- [29] R. M. Lutchyn, P. Nagornykh, and V. M. Yakovenko, Frequency and temperature dependence of the anomalous ac hall conductivity in a chiral $p_x + ip_y$ superconductor with impurities, *Phys. Rev. B* **80**, 104508 (2009).
- [30] E. Taylor and C. Kallin, Intrinsic hall effect in a multiband chiral superconductor in the absence of an external magnetic field, *Phys. Rev. Lett.* **108**, 157001 (2012).
- [31] K. I. Wysokiński, J. F. Annett, and B. L. Györfy, Intrinsic optical dichroism in the chiral superconducting state of Sr_2RuO_4 , *Phys. Rev. Lett.* **108**, 077004 (2012).
- [32] E. Taylor and C. Kallin, Anomalous hall conductivity of clean Sr_2RuO_4 at finite temperatures, *Journal of Physics: Conference Series* **449**, 012036 (2013).
- [33] M. Gradhand, K. I. Wysokiński, J. F. Annett, and B. L. Györfy, Kerr rotation in the unconventional superconductor Sr_2RuO_4 , *Phys. Rev. B* **88**, 094504 (2013).
- [34] J. Robbins, J. F. Annett, and M. Gradhand, Effect of spin-orbit coupling on the polar kerr effect in Sr_2RuO_4 , *Phys. Rev. B* **96**, 144503 (2017).
- [35] E. J. König and A. Levchenko, Kerr effect from diffractive skew scattering in chiral $p_x \pm ip_y$ superconductors, *Phys. Rev. Lett.* **118**, 027001 (2017).
- [36] M. D. E. Denys and P. M. R. Brydon, Origin of the anomalous hall effect in two-band chiral superconductors, *Phys. Rev. B* **103**, 094503 (2021).
- [37] H.-T. Liu, W. Chen, and W. Huang, Impact of random impurities on the anomalous hall effect in chiral superconductors, *Phys. Rev. B* **107**, 224517 (2023).
- [38] M. Yazdani-Hamid, M. Biderang, and A. Akbari, Polar kerr effect in multiband spin-orbit coupled superconductors, *Phys. Rev. B* **109**, 094510 (2024).
- [39] J.-L. Zhang, W. Chen, H.-T. Liu, Y. Li, Z. Wang, and W. Huang, Quantum-geometry-induced anomalous hall effect in nonunitary superconductors and application to Sr_2RuO_4 , *Phys. Rev. Lett.* **132**, 136001 (2024).
- [40] S. Ghosh, T. G. Kiely, A. Shekhter, F. Jerzembeck, N. Kikugawa, D. A. Sokolov, A. P. Mackenzie, and B. J. Ramshaw, Strong increase in ultrasound attenuation below T_c in Sr_2RuO_4 : Possible evidence for domains, *Phys. Rev. B* **106**, 024520 (2022).
- [41] H. M. L. Noad, K. Ishida, Y.-S. Li, E. Gati, V. Stangier, N. Kikugawa, D. A. Sokolov, M. Nicklas, B. Kim, I. I. Mazin, M. Garst, J. Schmalian, A. P. Mackenzie, and C. W. Hicks, Giant lattice softening at a lifshitz transition in Sr_2RuO_4 , *Science* **382**, 447 (2023).
- [42] P.-Y. Yang, H. M. L. Noad, M. E. Barber, N. Kikugawa, D. A. Sokolov, A. P. Mackenzie, and C. W. Hicks, Probing momentum-dependent scattering in uniaxially stressed Sr_2RuO_4 through the hall effect, *Phys. Rev. Lett.* **131**, 036301 (2023).
- [43] E. Abarca Morales, G.-R. Siemann, A. Zivanovic, P. A. E. Murgatroyd, I. Marković, B. Edwards, C. A. Hooley, D. A. Sokolov, N. Kikugawa, C. Cacho, M. D. Watson, T. K. Kim, C. W. Hicks, A. P. Mackenzie, and P. D. C. King, Hierarchy of lifshitz transitions in the surface electronic structure of Sr_2RuO_4 under uniaxial compression, *Phys. Rev. Lett.* **130**, 096401 (2023).
- [44] M. W. Haverkort, I. S. Elfimov, L. H. Tjeng, G. A. Sawatzky, and A. Damascelli, Strong spin-orbit coupling effects on the fermi surface of Sr_2RuO_4 and Sr_2RhO_4 , *Phys. Rev. Lett.* **101**, 026406 (2008).
- [45] O. Gingras, R. Nourafkan, A.-M. S. Tremblay, and M. Côté, Superconducting symmetries of Sr_2RuO_4 from first-principles electronic structure, *Phys. Rev. Lett.* **123**, 217005 (2019).
- [46] T. Scaffidi, Degeneracy between even- and odd-parity superconductivity in the quasi-one-dimensional hubbard model and implications for Sr_2RuO_4 , *Phys. Rev. B* **107**, 014505 (2023).
- [47] T. Nomura and K. Yamada, Detailed investigation of gap structure and specific heat in the p-wave superconductor Sr_2RuO_4 , *Journal of the Physical Society of Japan* **71**, 404 (2002).
- [48] A. Akbari and P. Thalmeier, Multiorbital and hybridization effects in the quasiparticle interference of the triplet superconductor Sr_2RuO_4 , *Phys. Rev. B* **88**, 134519 (2013).
- [49] B. Zinkl, M. H. Fischer, and M. Sigrist, Superconducting gap anisotropy and topological singularities due to lattice translational symmetry and their thermodynamic signatures, *Phys. Rev. B* **100**, 014519 (2019).
- [50] Y. Yu, S. Brown, S. Raghun, and K. Yang, Critical temperature T_c and pauli limited critical field of Sr_2RuO_4 : Uniaxial strain dependence, *Phys. Rev. B* **102**, 014509 (2020).
- [51] T. Salamone, H. G. Hugdal, S. H. Jacobsen, and M. Amundsen, High magnetic field superconductivity in a two-band superconductor, *Phys. Rev. B* **107**, 174516 (2023).
- [52] S. A. Kivelson, A. C. Yuan, B. Ramshaw, and R. Thomale, A proposal for reconciling diverse experiments on the superconducting state in Sr_2RuO_4 , *npj Quantum Materials* **5**, 43 (2020).
- [53] A. T. Rømer, D. D. Scherer, I. M. Eremin, P. J. Hirschfeld, and B. M. Andersen, Knight shift and leading superconducting instability from spin fluctuations in Sr_2RuO_4 , *Phys. Rev. Lett.* **123**, 247001 (2019).
- [54] A. Furusaki, M. Matsumoto, and M. Sigrist, Spontaneous hall effect in a chiral p-wave superconductor, *Phys. Rev. B* **64**, 054514 (2001).
- [55] N. P. Ong, Geometric interpretation of the weak-field hall conductivity in two-dimensional metals with arbitrary fermi surface, *Phys. Rev. B* **43**, 193 (1991).
- [56] K. Masuda and S. Kurihara, Coherence effect in a two-band superconductor: Application to iron pnictides, *Journal of the Physical Society of Japan* **79**, 074710 (2010).
- [57] B. Dóra, K. Maki, and A. Virosztek, Optical conductivity of

- superconducting Sr_2RuO_4 , **62**, 426 (2003).
- [58] S. Raghu, S. B. Chung, and S. Lederer, Theory of 'hidden' quasi-1d superconductivity in Sr_2RuO_4 , *Journal of Physics: Conference Series* **449**, 012031 (2013).
- [59] D. L. Maslov and A. V. Chubukov, Optical response of correlated electron systems, *Reports on Progress in Physics* **80**, 026503 (2016).
- [60] K. Oda, K. K. Tanaka, S. Onari, and M. Ichioka, Paramagnetic pair-breaking in spin-triplet superconductors with spin-orbit coupling: Application to Sr_2RuO_4 , *Journal of the Physical Society of Japan* **88**, 064707 (2019).